Rheology of Natural Sediments and Its Influence on the Settling of Dropstones in Hemipelagic Marine Sediment

E. Knappe, M. Manga, A. Le Friant

Rheology of natural sediments and its influence on the settling of dropstones in marine hemipelagic sediment

E. Knappe[1,2], M.Manga[1], A. Le Friant[3] and the IODP 340 scientists

[1] University of California at Berkeley, Department of Earth and Planetary Science

[2]University of Montana, Geoscience Department

[3]Insitut de Physique du Globe de Paris, Sorbonne Paris Cite

Corresponding author: Michael Manga (manga@seismo.berkeley.edu)

Key Points:

- We obtain a new dataset of rheology measurements from naturally occurring hemipelagic sediment and a terrestrial mud volcano
- Comparison with existing measurements indicates that particle composition influences yield stress and consistency.
- Most pumice clasts recovered from IODP 340 are stratigraphically in place and thus date the occurrence of eruptions.

Abstract

We investigate the rheology of naturally occurring hemipelagic marine sediment and compare measurements to another naturally occurring sediment from a terrestrial mud volcano and literature values. The hemipelagic marine sediment, collected by IODP 340, has a median grain size of 5.5 microns, is poorly sorted, and contains 31% clay, including smectite. The yield stresses and consistency are calculated by applying a range of shear stresses and shear-rates using a cone-and-plate rheometer. A Herschel-Bulkley model is fit to measured shear stresses and shear rates to calculate the yield stress and consistency. These measurements are performed at a range of particle concentrations and show that the hemipelagic sediment has a yield stress at particle concentrations as low as 10%. Increasing particle concentration increases the yield stress and consistency. We apply our results to show that natural pumice clasts need to have a radius greater than about 1 cm in order to settle through hemipelagic sediment on the sea floor. Most recovered pumice clasts from IODP 340 are thus preserved in the same horizon in which they were deposited.

1 Introduction

The rheological properties of sediment are influenced by multiple factors including particle concentration, size, size distribution, composition and pore-water salinity (Imran et al., 2001). Models for sediment rheology are often based on laboratory characterization of idealized kaolinite and montmorillonite mixtures (e.g. Maar et al., 2001; Baas and Best, 2002; Talling, 2013). These idealized mixtures differ from naturally occurring submarine sediment in particle size and distribution as well as composition. However, there are few studies of the rheology of natural submarine deposits (e.g., Imran et al., 2001; Locat et al., 2004; Jeong, 2013; Menapace et al., 2019).

41 The composition of the sediment can affect its rheology and cohesive sediments exhibit
42 complex behaviors that are often difficult to characterize (Yang et al., 2014). When materials
43 contain high clay fractions, strong attractive colloidal forces can lead to thixotropic behavior,
44 that is, the viscosity of the material depends on the shear history (Santolo et al., 2005).
45 Thixotropy is caused by a time dependent microstructural evolution of a material. When a shear
46 stress or strain is applied to the material the viscosity decreases (Barnes, 1997). In sediment, this
47 decrease in viscosity could be caused by the particles developing a preferred orientation or by the
48 breakdown of flocs and aggregates which release entrapped fluid and increases the lubrication
49 between the particles (Barnes, 1997; Tregger et al., 2010). However, this evolution is reversible:
50 the longer a material is at rest, the more the microstructure rebuilds until it reaches its initial state
51 again.

52 In addition to the clay fraction, the type of clay can also influence rheology due to
53 differences in cohesion. Smectite and montmorillonite have high cohesion compared to kaolinite
54 and illite. The difference in cohesion affects how easily the microstructure can be broken down.
55 Naturally occurring sediments differ from idealized mixtures because they contain a range of
56 sediment sizes, fossils, minerals and clays.

57 Thixotropy is also influenced by salinity and particle concentration. At high salinity,
58 greater than 0.35 g/l to 0.55 g/l, the inter-particle forces are strong enough to favor fast
59 reconstruction of the microstructure, thus making the material strongly thixotropic (Perret et al.,
60 1996). Particle concentration also affects the thixotropic behavior of a material. At low particle
61 concentrations, there are fewer interactions between the particles and thixotropic effects are less
62 significant (Santolo et al., 2012).

63 The rheological behavior of sediment has implications for the initiation and flow of
64 submarine sediment-laden density currents. Additionally, seafloor sediment preserves a record of
65 volcanic eruptions in tephra and crypto-tephra layers including isolated cm-sized pumice clasts
66 that record the occurrence of additional volcanic eruptions (le Friant et al., 2013, 2015; Palmer et
67 al., 2016; Jutzeler et al., 2016). These eruptions can be dated using the surrounding sediments but
68 this assumes that the clasts are at the same stratigraphic location and did not settle through
69 underlying sediment upon deposition.

70 In this study we analyze naturally occurring hemipelagic sediment collected from the
71 seafloor adjacent to Lesser Antilles Volcanic Arc. To determine yield stress and consistency as a
72 function of particle concentration a suite of rheometric tests are utilized. The yield stress and
73 consistency of a material depend strongly on the particle concentration. As particle concentration
74 increases, there is an increase in particle-particle interactions, which causes an increase in the
75 friction and thus increases the yield stress and consistency (Coussot and Piau, 1994). We thus
76 use a range of particle concentrations to develop a better understanding of how these natural
77 sediments flow. The same tests are performed on an additional naturally occurring sediment from
78 the Davis-Schrimpf mud volcanoes for further comparison. Additionally, our results are
79 compared to previously published measurements on other materials in order to better identify the
80 factors that influence rheology. For illustrative purposes, we use our results to determine the size
81 of particles that would settle through the hemipelagic sediment on the seafloor and hence what
82 size particles would be preserved in situ within marine sediments. We use these results to assess
83 whether volcanic dropstones collected by IODP 340 are preserved in situ.
84

85 **2 Methods**

The hemipelagic sediment was collected offshore of the Lesser Antilles volcanic arc from a water depth of 2745 meters. The Lesser Antilles volcanic arc is located at the eastern border of the Caribbean plate. The proximity of our sampling location to volcanic islands, specifically the active volcano Montagne Pelée, causes our sample to contain volcaniclastic sediment as well as marine fossils (le Friant et al., 2008). The sample, 340 U1400C 3H 4, was collected during IODP 340 from 26 meters below the sea floor from a sedimentary unit that includes multiple landslide deposits (le Friant et al., 2013; Lafuerza et al., 2015; Brunet et al., 2016); see supplementary Figure S1a for a location map. For comparison, another natural mud from the Davis-Schrimpf mud volcanoes located next to the Salton Sea in the Imperial Valley, California is analyzed (map in supplementary Figure S1b). The Salton Sea mud volcanoes are driven by the ascent of CO_2 from underlying geothermal systems and the mud recirculates within the subsurface plumbing system (Svenson et al., 2009).

2.1 Sample Properties

Size distribution is measured using a Sequoia Portable XR Laser Diffraction Particle Size Analyzer. The cumulative size distribution for both samples is shown in Figure 1a. The median grain size for the hemipelagic sediment is 5.5 microns. Grain density was measured as 2700 kg/m^3 on the IODP ship using helium pycnometry (le Friant et al., 2013).

Particle concentration, the amount of solids in the total mixture, is given by

$$\phi = \frac{V_s}{V_t} \quad (1)$$

where V_s the volume of solids, and V_t is the total volume. We measure ϕ by weighing a known volume of material. Uncertainty in ϕ is dominated by uncertainty in measured volume. The density of the hemipelagic sediment was confirmed to be 2700 kg/m^3.

Figure 1b,c shows three dimensional x-ray microtomography reconstructions of the samples imaged at the Advanced Light Source 8.3.2 beamline, Lawrence Berkeley National Laboratory, with a resolution of 1.3 microns/pixel. The hemipelagic marine sediment is poorly sorted and contains large voids (Figure 1b). Additionally, the sediment also contains foraminifera fossils and crystal fragments, such as hornblende, quartz and muscovite, that are large compared to particles in the surrounding matrix. The Salton Sea sediment has a more uniform size distribution by comparison (Figure 1c).

Using x-ray diffraction, we determine that the hemipelagic sediment is composed of 20% feldspar and plagioclase, 19% calcite, 16% quartz, 7% aragonite, and 31% clay. The Salton Sea sediment is composed of 41% quartz, 3% dolomite, 16% plagioclase, 8% orthoclase and 26% clay. The clay in both samples contains kaolinite, illite, and montmorillonite while the hemipelagic sediment also contains smectite.

3 Rheology Measurement Methods

We measure the rheology using a HAAKE Rheoscope 1. To ensure uniform strain-rate through the sample a cone and plate geometry, with a 4° cone angle and 60 mm diameter plate, is used. We apply either a controlled angular velocity, and hence a shear rate, and then measure the torque required to maintain this rate, or alternatively apply a torque and measure the resulting deformation.

In order to prevent slippage, both the cone and the plate are covered in ANSI 150 grit sand paper (average particle size of 100 microns). The gap size between the plate and the center of the cone was 0.142 mm after adhesion of sand paper. Each test utilizes 8ml of sample. To prevent jamming of particles within the gap, the mud is sieved to remove particles larger than

100 microns, which comprise less than a few percent of the volume of the sediment. The volumetrically dominant fine particles have a larger controlling influence on the yield stress, so we do not expect that the small number of fossils removed from the sample would alter the rheology (Yu et al., 2013). In order to prevent temperature fluctuations from affecting the measurements, the temperature of the mud is kept constant at 20°C using a Thermo Scientific Haake DC30-K20 Digital Bath. At this temperature water viscosity is 1.05 mPa s compared to 1.57 mPa s at a seafloor temperature of 4 °C.

The hemipelagic sediment is from a marine setting so we control salinity of the water by adding artificial seawater since the salinity of the water affects suspension rheology (Jeong, 2010). 35 grams of Instant Ocean salt mixture is added to 1 liter of water to create salinity similar to that of the Caribbean Sea.

The thixotropic nature of the sediment led us to focus on the static yield stress, above which the material will start to flow, and the dynamic yield stress, below which the material will no longer flow. Two separate tests are performed: the first to quantify the static yield and the second to determine the dynamic yield and consistency.

3.1 Flow Characteristics

In order to characterize rheology we consider an idealized constitutive model. The most frequently used model to describe naturally occurring sediments and muds is the Herschel-Bulkley model (Huang and Garcia, 1998):

$$\tau = \tau_y + K\dot{\gamma}^{\,n} \quad (2)$$

where τ is shear stress, τ_y is the yield stress, $\dot{\gamma}$ is strain rate, K is consistency, and n is the flow index. We adopt the Herschel-Bulkley model, but note that models without a yield stress have

also been used to model mud rheology especially for low strain rates and high viscosities (e.g., Menapace et al., 2019).

During the measurements, it became apparent that both materials did not simply follow the Herschel-Bulkley model (Supplementary Figure S2) as has been documented previously (e.g., Yang et al., 2014). Different stresses are measured when applying increasing and decreasing strain rates, indicating that the properties are history dependent, one signature of thixotropic rheology (Moller et al., 2009) (Supplementary Figure 2b). This leads to the static yield stress, which is associated with the start of flow, being higher than the dynamic yield stress, below which the material will stop flowing, due to the static yield stress having to breakdown the microstructure that has formed while the material was at rest. The microstructure breakdown is reversible; if the material is left at rest, the yield stress will increase again (Moller et al., 2009). There are models that quantify the evolving microstructure (e.g., Dullaert and Mewis, 2006; de Souza Mendes, 2009), however for this study we focus on the static yield stress and the dynamic yield stress. Consistency is analogous to viscosity, and is also quantified prior to the cessation of flow.

3.2 Static Yield

Thixotropic fluids have a viscosity that decreases over time as they are sheared. To mitigate the variations in shear history, samples are allowed to rest for ten minutes between each test (Van Kessel and Blom, 1998). After running hysteresis tests at varying time intervals between tests, the material recovers most of its strength after 10 minutes. Ten minutes limits the amount of evaporation of water and settling of particles so as to not affect measurements. Static yield is measured using a controlled stress mode while the sample was maintained at a constant

178 temperature. For this controlled stress mode, an increasing shear stress, τ, or torque, is applied
179 and the resulting deformation is measured (Supplementary Figure S2a). Shear stress is increased
180 linearly in 70 steps from 0 Pa to 1500 Pa, for 10 seconds each step. Initially, strain increases
181 linearly with stress, however with further increases of stress the strain grows exponentially fast
182 and is immeasurable after a certain shear stress. The location of this exponential increase varied
183 with each test depending on the water content. To calculate static yield stress a Herschel-Bulkley
184 model is fit to the data from increasing portion of the test, providing τ_y, K, and n.
185
186 **3.3 Dynamic Yield**
187 In order to determine the dynamic yield stress and the consistency, a shear strain rate, $\dot{\gamma}$,
188 is applied and the torque, or shear stress, τ, required to maintain this strain rate is measured.
189 Strain rate is increased in 40 steps uniformly spaced in the log of strain rate from 0.01 s^{-1} to 1.5 s^{-1}
190 , and subsequently decreased in the same 40 steps, with each step lasting 15 seconds
191 (Supplementary Figure S3 shows results for two different particle concentrations). To determine
192 the dynamic yield stress and consistency, the decreasing portion of the test is fit with a Bingham
193 model.
194
195 **4 Results**
196 Figure 2a shows the relationship between particle concentration (%) and yield stress (Pa)
197 for our samples compared to other studies. For the hemipelagic sediment and Salton Sea mud,
198 the filled circles show static yield stress and the open circles show dynamic yield stress. Table 1
199 summarizes the results for our study and Supplementary Table 1 summarizes comparative
200 studies. In our samples the dynamic yield stress is always lower than the static yield stress, with

the exception of the Salton Sea mud at a concentration of 40.5%. This exception could be the result of sedimentation within the sample that allowed the material to start flowing at a lower static yield stress. In addition to measuring the static yield using a controlled stress mode, we can estimate the static yield from the inflection point of the increasing strain rate portion of the dynamic yield tests (Santolo et al., 2012), and the two separately determined yield stresses are similar.

A yield stress becomes apparent in the hemipelagic sediment at a particle concentration of ~10% and increases with increasing particle concentration. Figure 2a also shows the yield stress as a function of particle concentration measured in other studies (Coussot and Piau, 1994; Coussot et al., 1996; Huang and Garcia, 1998; Matel et al., 2005; Remaitre et al., 2005; Maciel et al., 2009; Santolo et al., 2010; Blasio et al., 2010; Manga and Bonini, 2012; Jeong et al., 2013; Yang et al., 2014; Tran et al., 2014). In Figure 2, non-natural sediments are represented with squares.

To determine the yield stress as a function of particle concentration, the hemipelagic data is fit with the model developed by Mueller et al. (2009):

$$\tau_y = \tau^* \left(\left(1 - \frac{\phi}{\phi_m} \right)^{-2} - 1 \right) \quad (3)$$

where τ^* is a fitting parameter, ϕ is the particle concentration, ϕ_m is the maximum particle concentration. The fit of the Mueller et al. (2009) model to the hemipelagic static yield data is shown in Supplementary Figure 4. We find $\tau^* = 34.9 \pm 6.9$ Pa and $\phi_m = 0.23 \pm 0.004$.

Consistency also increases with increasing particle concentration. Following Mader et al. (2013), the hemipelagic data is fit to the model:

$$K_r = \left(1 - \frac{\phi}{\phi_m} \right)^{-2} \quad (4)$$

where $K_r = K/\mu_0$ where μ_0 is viscosity of the suspending fluid (Pa•s) (Supplementary Figure 5). We fnd $\phi_m = 0.25 \pm 0.02$ Pa and $\mu_0 = 0.14 \pm 0.05$ Pa s.

5 Discussion

Both the static and dynamic yield tests indicate that the hemipelagic sediment is thixotropic. In the dynamic tests, there is a significant difference between the increasing strain rate section and the decreasing strain rate section (Supplement 2b). This indicates that the material has a history dependence in its rheology and hence its microstructure. The higher the particle concentration, the more dramatic this hysteresis. In the static yield tests, the material initially behaves like a linear elastic material until a specific stress is overcome and then the strain exponentially increases until the material reaches another critical point and flows too fast for the rheometer to measure (Supplement 2a). Coussot et al. (1992) similarly found that the response of their clay-rich material is essentially elastic until a critical point is reached and the flow becomes unstable and fast. This behavior indicates that the material is initially structured, but when the apparent yield stress is overcome the sediment becomes unstructured and starts to flow at increasing velocities. Alignment of particles with the flow causes the material to flow faster when a shear is applied (Barnes, 1997). Additionally, the static yield stress is significantly larger than the dynamic yield stress, which is consistent with thixotropic behavior (Figure 2).

The scatter within our data could be caused by the history dependence of our samples due to slightly different handling of the material prior to testing. We tried to mitigate this effect by allowing the samples to rest between tests and by loading the samples into the rheometer in the same way. The scatter could additionally be caused by heterogeneities within the natural sample as each data point was obtained from a different aliquot of the mud.

246 The range of particle concentrations over which a yield stress can be measured for the
247 hemipelagic sediment is approximately between 10-20%. Below a concentration of 10% the
248 particles settle creating a muddy fluid top layer and particle rich layer underneath. Comparing
249 the results with other studies that used sediment suspensions, the hemipelagic marine sediment is
250 able to develop a static stress at comparatively low particle concentrations (Figure 2a).
251 Additionally, other studies that measured yield stresses at low particle concentrations were
252 kaolinite and water mixtures produced in the lab (Figure 2a – laboratory produced mixtures are
253 represented with squares).

254 The clay content in the hemipelagic sediment is in the higher range compared to the other
255 studies shown in Figure 2a, although not all studies record clay content. The hemipelagic
256 sediment has approximately 31% clay, which could be one of the contributing factors to why
257 there is a yield stresses at such low particle concentrations. Huang and García (1998) measure a
258 yield stress at lower concentration, approximately 7%, but do not record the clay content of the
259 sample they used. The higher clay content increases electrostatic forces between the clay
260 particles. Yu et al. (2013) found that increasing the clay content from approximately 10% to 40%
261 clay increased the yield stress by more than an order of magnitude, consistent with Jeong (2013)
262 who reported the highest clay content and similarly large yield stresses. While both the
263 hemipelagic sediment and Salton Sea mud have kaolinite, illite, montmorillonite, the
264 hemipelagic sediment also contains smectite, which is highly cohesive. The addition of this clay
265 type could also contribute to the higher yield stress and more thixotropic behavior compared to
266 the Salton Sea mud. The yield stress of the hemipelagic sediment is also more than an order of
267 magnitude larger than kaolinite suspensions with similar particle concentrations suggesting that

the presence of smectite is largely responsible for the higher yield stress (in Figure 2, compare Huang and Garcia (1998) and Maciel et al. (2009) data with the present measurements).

The salinity of the hemipelagic marine sediment, at 35 g/l, is well above the salinity that Perret et al. (1996) identify as influencing rheology. Above this salinity, there is fast reconstruction of the microstructure, and below the material is likely to favor slower reconstruction. Yang et al. (2014), however, found no effect on rheology of salinity in the range of fresh water to 50 g/L salinity. Using the method outlined by Perret et al. (1996) to determine the thixotropic nature of a material, the area between the hemipelagic sediment thixotropy test curves is larger than that of the Salton Sea sediment, indicating that the hemipelagic material is slower to recover back to its initial state. This indicates that the clay content has a larger effect than salinity for the two samples we considered.

Materials with high clay contents have a slow rate of reconstruction, increasing their recovery time (Barnes 1997). This is also the case for the two samples we considered. While the Salton Sea mud has a significant portion of clay, the median particle size of the hemipelagic sediment is much smaller at 5.5 microns, compared to the Salton Sea sediment 35.7 microns, which could account for the difference in recovery times.

5.1 Particle Settling through seafloor sediment

Hemipelagic sediment often contains isolated “dropstones” delivered by melting icebergs or volcanic eruptions; in the case of sediments offshore the Lesser Antilles volcanic arc, these are predominately pumice clasts, deposited from rafts of pumice or fall out. Whether these clasts are preserved within their deposit or subsequently sink multiple clast diameters through underlying layers depends on their size and weight. In order to determine whether a larger particle with

radius R_0 can settle within mud, we approximate the clast as a completely submerged sphere. The force is

$$F = \frac{4}{3}\pi(\rho_s - \rho)R_0^3 g \quad (5)$$

where ρ_s is the density of the sphere (kg/m^3), ρ is the density of the mud, R_0 is the radius of the sphere (m), and g is gravity (m/s^2). The density of the sediment depends on the particle concentration (C_v), $\rho=1800 \cdot C_v+1000$ kg/m^3. The sphere will cause yielding of the mud and sink when the yield stress parameter

$$Y_g = \frac{2\tau_y \pi R_0^2}{F} \quad (6)$$

exceeds a critical value of 0.143 (Beris et al., 1985). Pumice is porous, between 60-80% porosity, and at the bottom of the seafloor these pores will be filled with water. The mean density was calculated assuming 60% porosity and using a glass density of 2700 kg/m^3. We use a dynamic yield stress because we assume the clasts are initially moving when they reach the seafloor. Using equation (6) and equation (3) to determine the yield stress as a function of particle concentration, we calculate the relationship between the particle concentration and the radius of a clasts that would settle through the sediment (Figure 3). Below this radius, clasts would not settle but instead be preserved in situ. Using an average mud concentration at the seafloor of 10% (Hamilton, 1976) a pumice clast would have to have a radius larger than about 1 centimeter to settle through uncompacted hemipelagic sediment. Most of the various volcanic dropstones collected during IODP 340 (le Friant et al., 2013; Jutzeler et al., 2016) are thus in place and their stratigraphic locations record the time of eruptions.

6 Conclusion

By studying the rheology of a naturally occurring mud we can better discern some of the influencing factors in rheology and thixotropic behavior. Particle concentration affects the yield stress and consistency, with increasing particle concentrations leading to increasing yield stresses and consistency. As particle concentration increases, the thixotropic behavior also increases and the material becomes more history dependent. The particle concentration of the material also dictates the sizes of clasts that can settle through seafloor sediment. Pumice clasts would need radii greater than ~1 cm to settle through the hemipelagic sediment, indicating that most pumice clasts collected in IODP 340 are stratigraphically in place. Finally, the high smectite clay content in the hemipelagic sediment leads to more attractive colloidal forces in the sample and appears to influence the yield stress and enhance the thixotropic nature of the material.

7 Acknowledgements

This research used samples provided by the Integrated Ocean Drilling Program (IODP). Funding for this research was provided by a Post Expedition Activity award. We thank ANR-13-BS06-0009, Labex UnivEarth and Interreg Caraibes PREST for funding. The dedication and hard work of entire staff and scientific party on the Joides Resolution contributed to the sampling and analyses that made the present measurements possible, in particular O. Ishizuka, and staff scientists N. Stroncik and A. Klaus. Additional support was provided from the National Science Foundation. Aaron Tran and Max Rudolph helped with the sampling and analysis of the Salton Sea muds. Laurel Larson provided the particle size analyzer. Dula Parkinson guided the XRay tomography and reconstruction, and beamtime was provided by the ALS at LBNL. Tim Teague performed the XRD measurements and analysis. Rheologic measurements are available on

https://github.com/eknappe/rheology_tech_reports. We thank two reviewers for constructive comments and suggestions.

8 References

Baas, J. H., Best, J. L. 2002, Turbulence modulation in clay-rich sediment-laden flows and some implications for sediment deposition. Journal of Sedimentary Research, Vol 72, No. 3.

Barnes, H. A. 1997, Thixotropy — a review. Journal of Non-Newtonian Fluid Mechanics, Vol. 70, pp. 1-33.

Beris, A. N., Tsamopoulos, J. A., Armstrong, R. C., Brown, R. A. 1985, Creeping motion of a sphere through a Bingham plastic. Journal of Fluid Mechanics, Vol. 158, pp. 219-244.

Blasio, F. V., Breien, H., Elverhøi, A. 2011, Modelling a cohesive-frictional debris flow: an experimental, theoretical and field-based study. Earth Surface Processes and Landforms, Vol. 36, pp. 753-766.

Brunet, M., A. Le Friant, G. Boudon, S. Lafuerza, P. Talling, M. Hornbach, O. Ishizuka, E. Lebas, H. Guyard, and IODP Expedition 340 Science Party (2016), Composition, geometry, and emplacement dynamics of a large volcanic island landslide offshore Martinique: From volcano flank- collapse to seafloor sediment failure?, Geochem. Geophys. Geosyst., 17-3, 699– 724, doi:10.1002/2015GC006034.

Coussot, P., Leonov, A. I., Piau, J. M. 1992, Rheologic modeling and peculiar properties of some debris flows, Proceedings of International Symposium on Erosion, Debris Flows and Environment in Mountain Regions, I.A.H.S. Publication 209, pp. 207-216.

Coussot, P., Piau, J. M. 1994, On the behavior of fine mud suspensions. Rheologica Acta, Vol. 33, pp. 175-184.

Coussot, P., Proust, S., Ancey, C. 1996, Rheological interpretation of deposits of yield stress Fluids. Journal of Non-Newtonian Fluid Mechanics, Vol. 66, pp. 55-70.

de Souza Mendes, P. R. 2009, Modeling the thixotropic behavior of structured fluids. Journal of Non-Newtonian Fluid Mechanics, Vol. 164, pp. 66-75.

Dullaert, K., Mewis, J. 2006, A structural kinetics model for thixotropy. Journal of Non-Newtonian Fluid Mechanics, Vol. 139, pp. 21-30.

Hamilton, E. L. 1976, Variations of density and porosity with depth in deep-sea sediments. Journal of Sedimentary Petrology, Vol. 46, pp. 280-300.

Huang, X., García, M. H. 1998, A Herschel-Bulkley model for mud flow down a slope. Journal of Fluid Mechanics, Vol. 374, pp. 305-333.

Imran, J., Parker, G., Locat, J., Lee, H. 2001, 1D Numerical model of muddy subaqueous and subaerial debris flows. Journal of Hydraulic Engineering, Vol. 127, pp. 959-968.

Jeong, S. W. 2010, Grain size dependent rheology on the mobility of debris flows. Geoscience Journal, Vol. 14, pp. 359-369.

Jeong, S. W. 2013, Determining the viscosity and yield surface of marine sediments using modified Bingham models. Geosciences Journal, Vol. 17, pp. 241-247.

Jutzeler, M., M. Manga, J.D.L. White, P.J. Talling, A.A. Proussevitch, S.F.L. Watt, M. Cassidy, R.N. Taylor, A. Le Friant, and O. Ishizuka (2016) Submarine deposits from pumice-rich pyroclastic density currents dispersing over water: an outstanding example from offshore Montserrat (IODP 340), *Bulletin of the Geological Society of America*, doi: dx.doi.org/20.1130/B31448.1

Lafuerza S., A. Le Friant, M. Manga, G. Boudon, B. Villemant, N. Stroncik, B. Voight, M. Hornbach, O. Ishizuka and the Expedition 340 Scientific Party. 2014, Geomechanical characterizations of submarine volcano flank sediments, Martinique, Lesse Antilles Arc. S. Krastel et al., (Eds.), Sumarine mass movements and consequences, *Advances in Natural and Technological Hazards Research,* Springer Inten. Publishing, Switzerland, 2014, 37, 73-81, doi 10.1007/978-3-319-00972-8_7.

Le Friant, A., Lock, E.J., Hart, M.B., Boudon, G., Sparks, R.S.J., Leng, M.J., Smart, C.W., Komorowski, J.C., Deplus, C., Fisher, J.K. 2008, Late Pleistocene tephrochronology of marine sediments adjacent to Montserrat, Lesser Antilles volcanic arc. Journal of rthe Geological Society, London, (London, U. K.), Vol. 165, pp. 279–289.

Le Friant, A., Ishizuka, O., Stroncik, N. A., and the Expedition 340 Scientists 2013, Lesser Antilles Volcanism and Landslides, Integrated Ocean Drilling Program Expedition 340 Preliminary Report, doi:10.2204.iodp.pr.340.2012.

Le Friant, A., Ishizuka, O. , Boudon, G. , Palmer, M.R. , Talling, P. , Villemant, B. , Adachi, T., Aljahdali, M., Breitkreuz, C., Brunet, M., Caron, B., Coussens, M., Deplus, C., Endo, D., Feuillet, N., Fraas, A.J., Fujinawa, A., Hart, M. B., Hatfield, R.G., Hornbach, M., Jutzeler, M., Kataoka, K. S., Komorowski, J-C., Lebas, E., Lafuerza, S., Maeno, F., Manga, M., Martínez-Colón, M., McCanta, M., Morgan, S., Saito, T., Slagle, A., Sparks, S., Stinton, A., Stroncik, N., Subramanyam, K. S.V., Tamura, Y., Trofimovs, J., Voight, B., Wall-Palmer, D., Wang, F., Watt, S.F.L. 2015, Submarine record of volcanic island construction and collapse in the Lesser Antilles arc: First scientific drilling of submarine volcanic island landslides by IODP Expedition 340. *Geochem., Geophys., Geosyst, 16*, 2, 420-442.

Locat, J, Lee, H.J., Locat, P., Imran, J. 2004, Numerical analysis of the mobility of the Palos Verdes debris avalanche, California, and its implication for the generation of tsunamis. Marine Geology, Vol. 203, pp. 269-280.

Maciel, G. F., Santos, H. K., Ferreira, F. O. 2009, Rheological Analysis of water clay compositions in order to investigate mudflows developing in canals. Journal of the Brazil Society of Mechanical Science and Engineer, 31, 64-74.

Mader, H.M., Llewellin, E. W., Mueller, S. P. 2013, The rheology of two-phase magmas: A review and analysis. Journal of Volcanology and Geothermal research, 257, 135-158.

Malet, J.P., Laigle, D., Remaitre, A., Maquaire, O. 2005, Triggering condition and mobility of debris flows associated to complex earthflow. Geomorphology, 66, 215-235.

Manga, M., Bonini, M. 2012, Large historical eruptions at subaerial mud volcanoes, Italy. Natural Hazards and Earth System Science, Vol. 12, pp. 3377-3386.

Menapace, W., Tangunan, D., Maas, M., Williams, T., Kopf, A. 2019, Rheology and biostratigraphy of the Maraian serpentine muds unravel mud volcano evolution. Journal of Geophysical Research, Vol. 124, doi.org/10.1029/2019JB018265.

Marr, J. G., Harff, P.A., Shanmugam, G., Parker, G. 2001. Experiments on subaqueous sandy gravity flows: The role of clay and water content in flow dynamics and depositional structures. GSA Bulletin, Vol. 113, No. 11, 1377-1386.

Moller, P., Fall, A., Chikkadi, V., Derks, D., Bonn, D. 2009, An attempt to categorize yield stress fluid behavior. Philosophical Transactions of the Royal Society, Vol. 367, pp. 5139-5155.

Mueller, S., Llewellin, E. W., Mader, H. M. 2009, The rheology of suspensions of solid particles. Proceedings of the Royal Society, Vol. 446, pp. 1201-1228.

Palmer, M., Hatter S.J., Gernon T.M., Taylor, R.N., Cassidy M., Johnson P., Le Friant A., Ishizuka, O., 2016, Discovery of a large 2.4 Ma Plinian eruption of Basse-Terre, Guadeloupe, from the marine sediment record. Geology, 44-2, 123-126, doi:10.1130/G37193.1

Perret, D., Locat, J., Martignoni, P. 1996, Thixotropic behavior during shear of a fine-grained mud from Eastern Canada. Engineering Geology, Vol. 43, pp. 31-44.

Remaitre, Al., Matel, J.P., Maquaire, O., Ancey, C., Locat, J. 2005, Flow behavior and runout modeling of a complex debris flow in a clay-shale basin. Earth Surface Processes and Landforms, 30, 479-488.

Santolo, A. S., Evangelista, A. 2005, Some observations on the prediction of the dynamic parameters of debris flows in pyroclastic deposits in the Campania region of Italy. Natural Hazards, Vol. 50, pp. 605-622.

Santolo, A. S., Pellegrino, A. M., Evangelista, A. 2010, Experimental study on the rheologic behavior of debris flow. Natural Hazards Earth System Science, Vol. 10, pp. 2507-2514.

Santolo, A. S., Pellegrino, A. M., Evangelista, A., Coussot, P. 2012, Rheologic behavior of reconstituted pyroclastic debris flow. Geotechnique, Vol. 62, pp. 19-27.

Svensen, H., Hammer, O., Mazzini, A., Onderdonk, N., Polteau S., Planke, S., Podladchikov, Y.Y. 2009, Dynamics of hydrothermal seeps from the Salton Sea geothermal system (California, USA) constrained by temperature monitoring and time series analysis. Journal of Geophysical Research, Vol. 114, B09201, doi:10.1029/2008JB006247.

Talling, P. J. 2013, Hybrid submarine flows comprising turbidity current and cohesive debris flow: Deposits, theoretical and experimental analyses and generalized models, Geosphere, Vol. 9, No. 3, doi: 10.1130/GES00793.

Tran, A., Rudolph, M.L., Manga, M. 2014, Bubble mobility in mud and yield stress fluids, submitted to Journal of Volcanology and Geothermal Research.

Tregger, N.A., Pakula, M. E., Shah, S. P. 2010, Influence of clays on the rheology of cement pastes. Cement and Concrete Research, Vol. 40, pp. 384-391.

Van Kessel T. and Blom C. 1998, Rheology of cohesive sediments: comparison between anatural and an artificial mud. Journal of Hydraulic Research, Vol. 36, pp. 591–612

Yang, W.Y., Yu, G.-L, Tan, S., Wang, H.K. 2014, Rheological properties of dense natural cohesive sediments subject to shear loadings. International Journal of Sediment Research, Vol. 29, pp. 454-470.

Yu, B., Ma, Y., Qi, X. 2013, Experimental study on the influence of clay mineral on the yield stress of debris flows. Journal of Hydraulic Engineering, Vol. 139, pp. 364-373.

Figure 1. a) The mean cumulative size distribution of the sediments. The hemipelagic sediment, shown in blue, is the average of four tests, and the Salton Sea sediment, shown in red, is the average of two tests. b) 3-D microtomography reconstructions of the materials. Reconstruction of the hemipelagic sediment, which is poorly sorted and contains large fossils. C) Reconstruction of the Salton Sea sediment, which is much more uniform in size than the hemipelagic sediment.

Figure 2. a) Yield stress as a function of particle concentration from multiple different studies, b) consistency as a function of particle concentration from multiple different studies. Clay contents shown in numbers next to the respective data when reported. For our measurements, open symbols show static yield stress and filled symbols show dynamic yield stress. All data in Table 1 and Supplementary Table 1.

Table 1. The hemipelagic sediment and Salton Sea sediment measured in this study. Includes the parameters used to fit the Herschel-Bulkley model. Data plotted in Figure 2.

Figure 3. Particle concentration of hemipelagic sediment and the clast radius that would exceed the yield stress parameter defined by Beris et al. (1985). For radii above the blue curve, clasts

516 will settle through the hemipelagic marine sediment. Clasts are approximated as spheres of
517 density 1.65 g/cm^3.
518

Figure 1.

a.

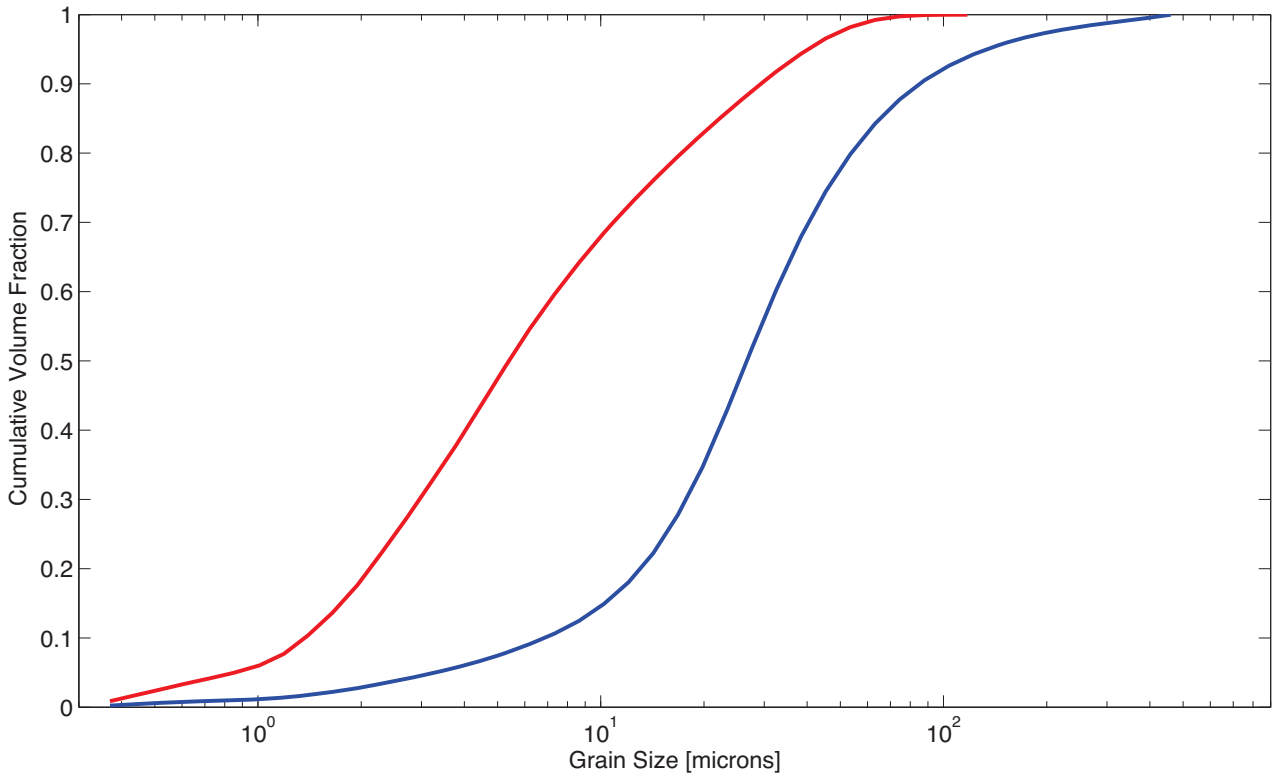
Cumulative Volume Fraction
Grain Size [microns]
0
0.1
0.2
0.3
0.4
0.5
0.6
0.7
0.8
0.9
1
10^0
10^1
10^2

b.

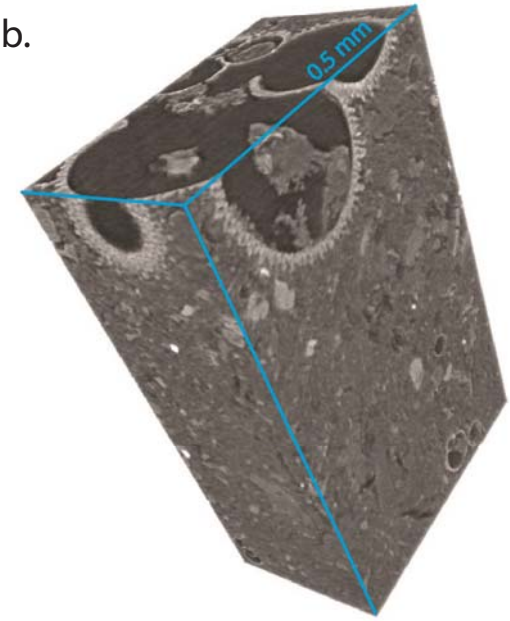
0.5 mm

c.

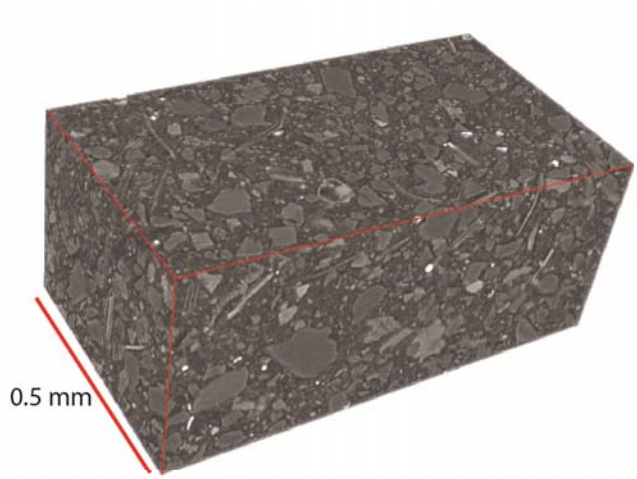
0.5 mm

Figure 2.

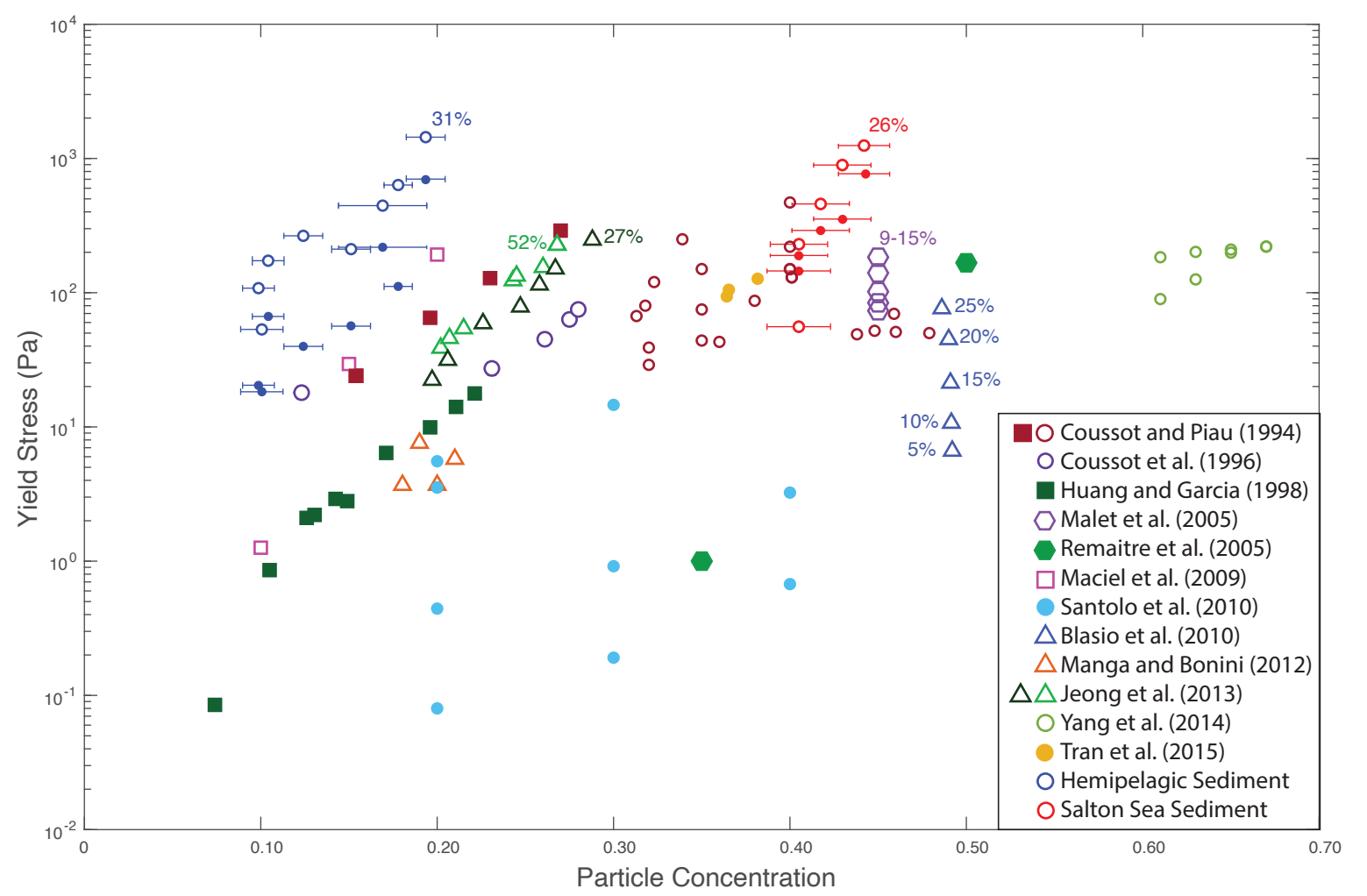
Yield Stress (Pa)
Particle Concentration
31%
26%
52%
27%
9-15%
25%
20%
15%
10%
5%
Coussot and Piau (1994)
Coussot et al. (1996)
Huang and Garcia (1998)
Malet et al. (2005)
Remaitre et al. (2005)
Maciel et al. (2009)
Santolo et al. (2010)
Blasio et al. (2010)
Manga and Bonini (2012)
Jeong et al. (2013)
Yang et al. (2014)
Tran et al. (2015)
Hemipelagic Sediment
Salton Sea Sediment

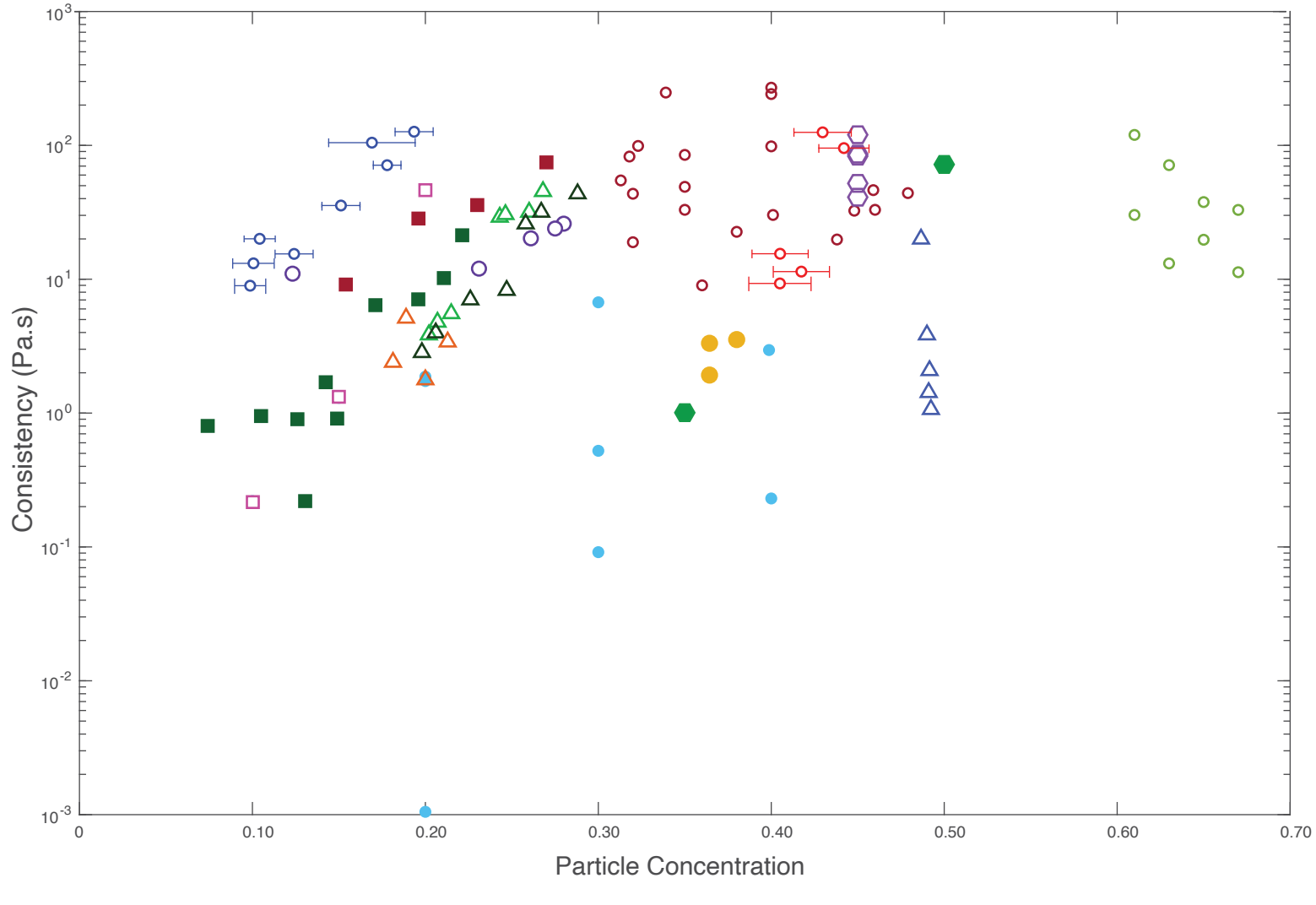
Consistency (Pa.s)
Particle Concentration

Sample	Particle Concentration (%)	Dynamic Yield (Pa)	Consistency (Pa·s)	Static Yield (Pa)
Hemipelagic Marine Sediment	19.4 ± 1.1%	701.9 ± 2.6	126.4 ± 5.8	1440.9 ± 1.5
	17.8 ± 0.8%	111.4 ± 2.8	71.1 ± 4.1	634.2 ± 17.4
	16.9 ± 2.5%	218.1 ± 2.1	104.8 ± 3.5	445.3 ± 13.9
	12.4 ± 1.1%	39.8 ± 0.2	15.5 ± 0.6	265.3 ± 3.2
	15.1 ± 1.1%	56.3 ± 0.7	35.5 ± 2.2	211.1 ± 9.4
	10.4 ± 0.9%	66.5 ± 0.3	20.0 ± 0.9	173.1 ± 5.6
	9.9 ± 0.9%	20.5 ± 0.6	8.9 ± 1.4	108.1 ± 7.3
	10.1 ± 1.2%	18.3 ± 0.5	13.1 ± 1.0	53.3 ± 3.9
Salton Sea Mud Volcano	44.2 ± 1.45%	769.1 ± 3.0	95.4 ± 22.3	1247.8 ± 2.6
	42.9 ± 1.6%	353.6 ± 0.7	125.1 ± 1.9	893.4 ± 0.2
	41.7 ± 1.6%	291.1 ± 0.8	11.4 ± 4.7	458.3 ± 0.9
	40.5 ± 1.6%	189.4 ± 0.9	15.5 ± 8.2	229.7 ± 11.1
	40.5 ± 1.8%	145.3 ± 0.5	9.3 ± 4.9	55.8 ± 20.1

Density (g/cm^3)	% Clay	n
1.34	31	3.5
1.31	31	3.5
1.29	31	3.5
1.22	31	3.5
1.27	31	4.5
1.18	31	3.5
1.17	31	3.6
1.18	31	3.5
1.76	26	3.5
1.73	26	3.5
1.7	26	3.5
1.67	26	3.5
1.68	26	3.5

Figure 3.

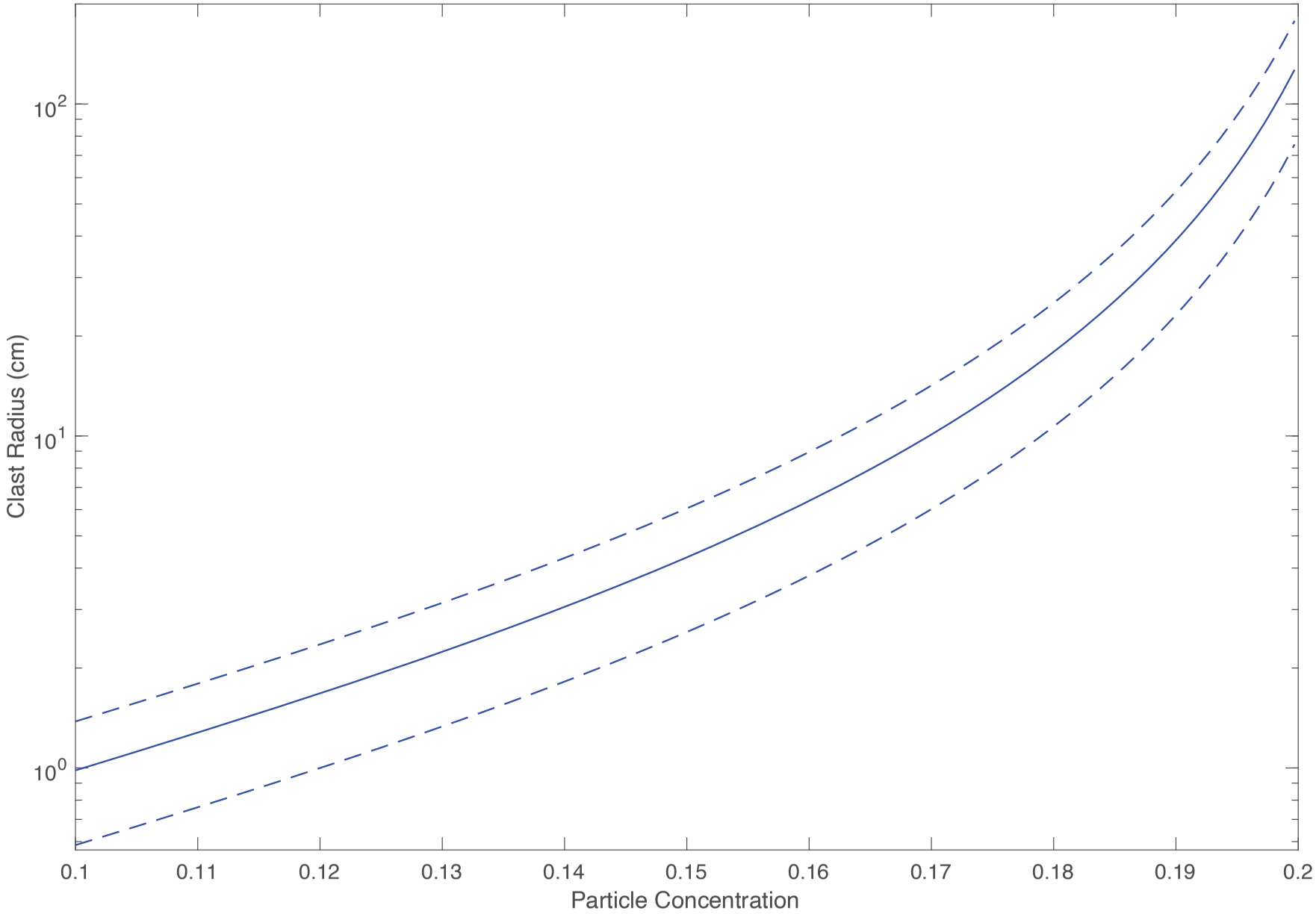
Clast Radius (cm)
10^2
10^1
10^0
0.1
0.11
0.12
0.13
0.14
0.15
0.16
0.17
0.18
0.19
0.2
Particle Concentration